
Static and Optical Properties of Warm Dense Polystyrene Along the Principal Hugoniot

Warm dense matter (WDM) occupies a critical regime within the physics branches more traditionally addressed by condensed matter and plasma physics. WDM has recently received considerable attention because of identification with environments as diverse as the interiors of exoplanets,¹ the atmospheres of stars,² inertial confinement fusion (ICF) capsules,³ and the plasma from laser interactions⁴ with materials. Broadly, WDM spans temperatures from a few tens to several hundred electron volts and densities from 10^{21} to 10^{25} atoms/cm³, covering conditions from melt to fully ionized plasmas. Modeling this regime presents a particularly difficult challenge given that quantum mechanical effects play a crucial role in accurately representing this complex medium under extreme conditions. In addition, many of these environments constitute the dynamic interplay between mixtures of species in various physical states. Because of this complexity, few systematic experimental studies have examined its nature. One exception is ICF, in which laser-powered shocks combined with accurate diagnostic tools have begun to penetrate its intricacies and provide detailed tests of various WDM theoretical models.

For example, hydrocarbon polymers such as polystyrene (CH) and glow-discharge-polymer (GDP) plastic are often used as the ablator material in inertial confinement targets, for both indirect-drive⁵ and direct-drive⁶ ICF configurations. In ICF implosions, the ablator materials are compressed into the WDM regime by shocks. Typically, the shocked ablators can have temperatures of $T = 5$ to 50 eV and densities of $2\times$ to $10\times$ solid density. Accurate knowledge of the ablator properties in the WDM regime is just as crucial for ICF designs as the properties of the deuterium-tritium (DT) fuel.^{7–14} The static equation of state (EOS) determines the material's compressibility,¹⁵ while the dynamic and optical properties affect the thermal and radiation transports in the material.^{16–18}

Because of their importance to ICF target designs, the properties of various polymers in the WDM regime have recently been extensively studied using laser-driven shock waves. In contrast to the previous gas-gun experiment¹⁹ in the low-pressure regime ($P < 1$ Mbar), an early Nova experi-

ment²⁰ showed a stiffer behavior of CH at pressures of 10 to 40 Mbar than the Hugoniot derived from the *SESAME*²¹ and “quotidian” equation-of-state (QEOS)²² models. This has stimulated more-recent experimental studies^{23–26} of the CH Hugoniot in the 1- to 10-Mbar regime. In addition to the Hugoniot pressure, the temperature and optical reflectivity of CH shocks have also been measured in some impedance-matching experiments using the velocity interferometer system for any reflector (VISAR).^{27,28} These high-quality experimental data could advance our understanding of the properties of shocked polymers.

In general, the theoretical exploration of material properties in the WDM regime remains difficult because of the co-existence of different species including electrons, ions, atoms, and molecules in strongly coupled and degenerate conditions. To simulate such complex systems, one must adopt first-principles methods such as quantum molecular dynamics (QMD),^{29–35} path-integral Monte Carlo (PIMC),^{36–39} and coupled electron-ion Monte Carlo (CEIMC)⁴⁰ methods. For example, using the QMD method, the principal shock Hugoniots of polyethylene,⁴¹ CH,⁴² and plastic²⁶ with a composition of CH_{1.36} have recently been investigated up to ~ 15 Mbar. Noticeable differences for CH_{1.36} in the pressure range have been observed when compared to the QEOS-based Livermore EOS prediction.²⁶ For CH, the previous QMD simulations (up to only ~ 8 Mbar) by Wang *et al.*⁴² showed good agreement with a recent OMEGA experiment²⁵ but failed to predict the measured reflectivity.

In this article, we employed the QMD method to investigate the principal Hugoniot of CH up to a very high pressure of 62 Mbar. The shock pressure and temperature from our QMD calculations agree very well with recent impedance-matching measurements ($P < 10$ Mbar) on OMEGA. When compared to the *SESAME* EOS model, a stiffer behavior in CH is predicted by QMD simulations at pressures above 10 Mbar. In addition, the reflectivity discrepancy seen in previous QMD simulations⁴² has been resolved. The present QMD calculations recover the measured reflectivity only when the proper refraction index n_0 of the unshocked CH is taken into account.

The structure change in CH at 1 to 2 Mbar has been found to be consistent with the turn-on of reflectivity in both experiment and QMD calculations.

The Vienna *ab initio* simulation package (VASP)^{43–45} was used for our QMD calculations within the isokinetic ensemble (particle/volume/temperature NVT constant). The VASP code is based on the finite-temperature density-functional theory (FTDFT) in which electrons are treated quantum-mechanically by a plane-wave basis within the generalized gradient approximation (GGA), using the Perdew–Burke–Ernzerhof (PBE) exchange-correlation function.⁴⁶ Projector augmented wave (PAW) pseudopotentials were used to account for the core electrons. To converge the energy and pressure calculations, we set the plane-wave cutoff energy to 1000 eV and adopted hard potentials with tight cores (core radii of 1.1 and 0.8 a.u. for C and H, respectively). The system was assumed to be in local thermodynamical equilibrium with equal electron and ion temperatures ($T_e = T_i$). A periodically replicated cubic cell was used with 125 atoms for each species of H and C, with the volume of the cell determined by the CH density. For each molecular dynamics (MD) step, a set of electronic-state functions for each k point was self-consistently determined for a given ionic configuration. Then, the ions were moved classically with a velocity Verlet algorithm, according to the combined ionic and electronic forces. The ion temperature was kept constant by a simple velocity scaling. A set of self-consistent ion trajectories and electronic-wave functions resulted from the MD time propagation. These trajectories provide a consistent set of static, dynamic, and optical properties of warm dense CH. The QMD calculations employed a Γ -point ($\mathbf{k} = 0$) sampling of the first Brillouin zone in the cubic cell. Testing with a $2 \times 2 \times 2$ Monkhorst–Pack k -point grid, we found that the resulting pressure and energy varied by only $\sim 2\%$. For the lowest

temperature point, we used 650 bands and a time step of $\Delta t = 0.5$ fs, while for the highest temperature points, we employed a larger number (8000) of bands and a smaller time step of $\Delta t = 0.0325$ fs. The correlation times varied slightly at 5.0 to 6.0 fs.

To search for the shock Hugoniot of CH at a given temperature, we performed QMD calculations for two close densities differing by only ~ 0.05 g/cm³. The obtained energy and pressure were used to evaluate how far the two calculated densities were from the true Hugoniot point, which is defined by the Hugoniot equation

$$\text{Hug} = E_f - E_0 + \frac{1}{2}(P_f + P_0) \times \left(\frac{1}{\rho_f} - \frac{1}{\rho_0} \right) = 0.$$

The pressure, internal energy, and density of the initial unshocked CH are characterized by (P_0, E_0, ρ_0) , while the shock has the quantities of (P_f, E_f, ρ_f) . The initial density used in the experiments was $\rho_0 = 1.05$ g/cm³. By linearly interpolating/extrapolating through the two calculated points to make $\text{Hug} \equiv 0$, we can determine the Hugoniot point (P_h, E_h, ρ_h) for the given temperature. The principal Hugoniot of CH is displayed in Table 138.VIII, in which the shock and particle velocities $[U_s = \sqrt{\rho_h(P_h - P_0)/(\rho_h \rho_0 - \rho_0^2)}$ and $U_p = (P_h - P_0)/(\rho_0 U_s)]$, respectively, are also given. The highest calculated pressure point reached an unprecedented level of $P \sim 62$ Mbar.

To explore the change of material structure along the principal Hugoniot, we have plotted the pair-correlation functions $g(r)$ in Fig. 138.43 among ions of (a) carbon–carbon, (b) carbon–hydrogen, and (c) hydrogen–hydrogen. Figure 138.43 displays calculations for two temperatures at $T = 5000$ K (solid red line) and $T = 15,000$ K (dashed blue line), corresponding to pressures of 0.914 Mbar and 2.198 Mbar, respectively. The peaks in $g(r)$ appearing at a low temperature of 5000 K wash out as

Table 138.VIII: The principal Hugoniot of polystyrene (CH) predicted by QMD calculations.

T (K)	ρ (g/cm ³)	P (Mbar)	U_s (km/s)	U_p (km/s)	ρ/ρ_0
2,000	1.941	0.264	6.966	3.198	1.848
5,000	2.551	0.914	11.961	7.037	2.429
15,000	2.938	2.198	17.924	11.519	2.798
30,000	3.139	3.872	23.448	15.605	2.990
60,000	3.379	7.370	31.848	21.951	3.218
90,000	3.561	11.392	39.174	27.624	3.392
120,000	3.681	15.698	45.691	32.659	3.506
220,000	3.959	31.468	63.835	46.904	3.770
400,000	4.136	62.406	89.230	66.575	3.939

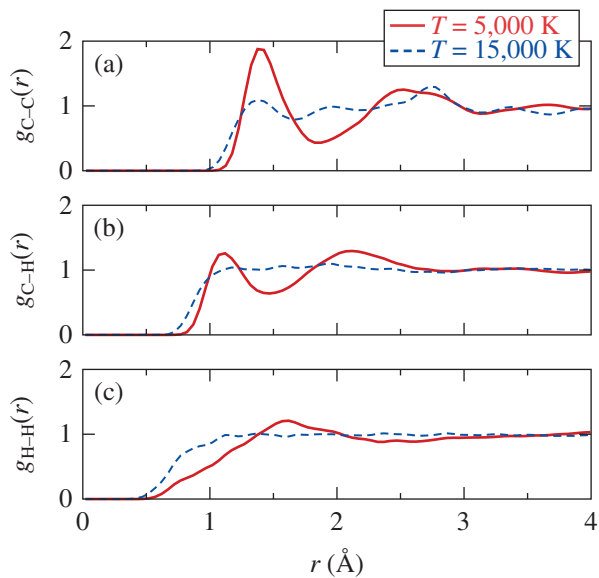


Figure 138.43

The QMD-predicted pair-correlation functions of shocked CH, along the principal Hugoniot at temperatures of $T = 5,000$ K (solid red line) and $T = 15,000$ K (dashed blue line) for (a) carbon–carbon, (b) carbon–hydrogen, and (c) hydrogen–hydrogen correlations.

the pressure increases to ~ 2 Mbar, indicating a change in the material structure around $P \simeq 1$ to 2 Mbar, which is found to be consistent with the turn-on of reflectivity (discussed below).

CH Hugoniot is compared with both experiments and models in Fig. 138.44 by plotting the pressure as a function of the shock density. The QMD results (red circles) are compared with a gas-gun experiment¹⁹ (purple triangles), a Nova experiment²⁰ (green diamonds), a recent OMEGA experiment²⁵ (blue squares), and the *SESAME* model²¹ (dashed–dotted line). It is noted that the OMEGA data have been corrected using the improved quartz standard.⁴⁷ Figure 138.44 shows that the QMD-predicted Hugoniot pressure of CH is in good agreement (within 6% or less) with recent OMEGA experiments and gas-gun experiments for pressures less than ~ 10 Mbar, in which the *SESAME* model is also close to both QMD and experiments. In the high-pressure regime ($P = 10$ to 62 Mbar), however, the QMD predictions indicate a slightly stiffer behavior than the *SESAME* model (*SESAME* 7593). For the highest pressure explored ($P \sim 62$ Mbar), the compression predicted by the QMD calculation is $\sim 5\%$ lower than what the *SESAME* model suggested. For the same density of $\rho = 4.1$ g/cm³, the QMD-predicted pressure of ~ 62 Mbar is higher than the 33 Mbar inferred from *SESAME*. It is not as stiff, however, as the early Nova experiment²⁰ indicated.

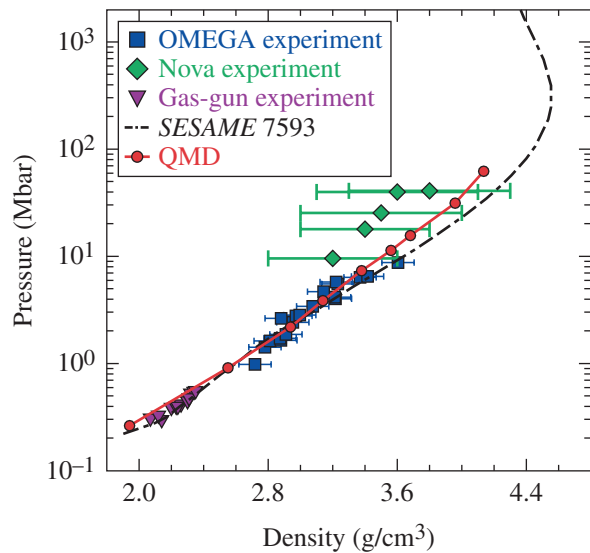


Figure 138.44

The pressure of shocked CH is plotted as a function of density, along the principal Hugoniot. The QMD results (red circles) are compared with a gas-gun experiment,¹⁹ a Nova experiment,²⁰ a recent impedance-matching experiment²⁵ on OMEGA, and *SESAME* model predictions.

In Fig. 138.45, the measured shock temperatures from the OMEGA experiment²⁵ are compared with both the QMD calculations and the *SESAME* model (*SESAME* 7593). It is found that the *SESAME* model slightly overestimates the shock temperature by $\sim 10\%$ for this low-pressure regime ($P < 10$ Mbar), while the QMD results reproduce the OMEGA measurement very well except for the highest data point. The highest data point, which has a higher temperature than both the QMD and *SESAME* predictions by 20% to 30%, might have been compromised by the normalization to that of the quartz standard.²⁵ A similar discrepancy for the highest data point was also observed in the previous QMD calculation⁴² by Wang *et al.*⁴² In the Fig. 138.45 inset, the comparison of shock temperature between QMD and the *SESAME* model has been extended to a wider range of pressures. The shock temperature predicted by QMD is higher than that of the *SESAME* model for pressures of $P > 20$ Mbar. This is consistent with the QMD-predicted stiffer behavior of CH for this high-pressure regime (see Fig. 138.44).

Finally, we examine the reflectivity of shocked CH along the principal Hugoniot. In both the OMEGA experiment²⁵ and a LULI experiment,²³ the reflectivity was determined by the signal level of the probe beam ($\lambda = 532$ nm) reflected by the CH

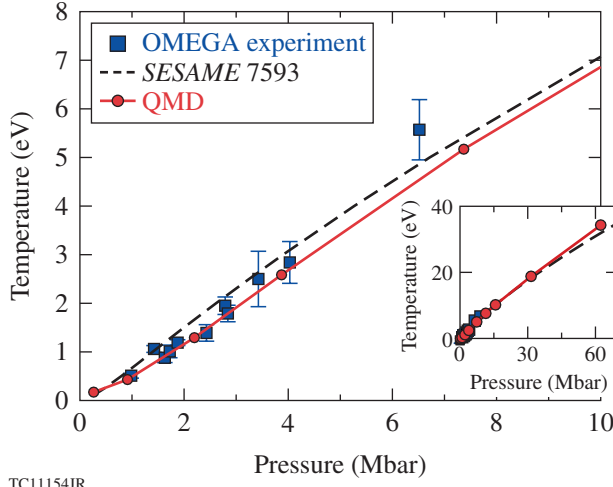


Figure 138.45

The shock temperature of CH is plotted as a function of pressure, along the principal Hugoniot. The QMD results (red circles) are compared with the recent impedance-matching experiment on OMEGA.²⁵ The inset shows the temperature comparison between the QMD prediction and the *SESAME* model to the entire explored pressure range.

shock front, which was detected by the VISAR streak camera. In the QMD calculations, we obtained a consistent set of trajectories of the ionic configuration during the molecular dynamics time propagation. We chose about ten uncorrelated snapshots of these configurations to calculate the velocity dipole matrix elements D_{mn} from the VASP wave functions. The quantity D_{mn} is used to compute the frequency-dependent Onsager coefficients within the Kubo–Greenwood formalism:⁴⁸

$$L_{ij}(\omega) = \sum_{mn} \frac{2\pi(-e)^{4-i-j}}{3Vm_e^2\omega} F_{mn} |D_{mn}|^2 \times \left(\frac{E_m + E_n}{2} - H \right)^{i+j-2} \delta(E_m - E_n - \hbar\omega), \quad (1)$$

where $V = 1/\rho$ is the atomic volume, $E_m(E_n)$ is the energy of the m th (n th) state, and H is the enthalpy (per atom) of the system. The quantity of F_{mn} is the difference between the Fermi–Dirac distributions for the m and n states at temperature T . In practical calculations, the δ function in the above equation is approximated by a Gaussian function of width ΔE ($\simeq 0.5$ eV). From the real part of the electric conductivity, $\sigma_1(\omega) = L_{11}(\omega)$, we obtain the imaginary part of the electric conductivity from a principal value integral:

$$\sigma_2(\omega) = -\frac{2}{\pi} P \left[\int \frac{\omega' \sigma_1(\omega')}{\omega'^2 - \omega^2} d\omega' \right]. \quad (2)$$

The dielectric function, $\epsilon(\omega) = \epsilon_1(\omega) + i\epsilon_2(\omega)$, can be calculated by

$$\begin{aligned} \epsilon_1(\omega) &= 1 - \frac{4\pi}{\omega} \sigma_2(\omega), \\ \epsilon_2(\omega) &= \frac{4\pi}{\omega} \sigma_1(\omega). \end{aligned} \quad (3)$$

Using the dielectric function, one obtains the real $[n(\omega)]$ and imaginary $[k(\omega)]$ parts of the refraction index:

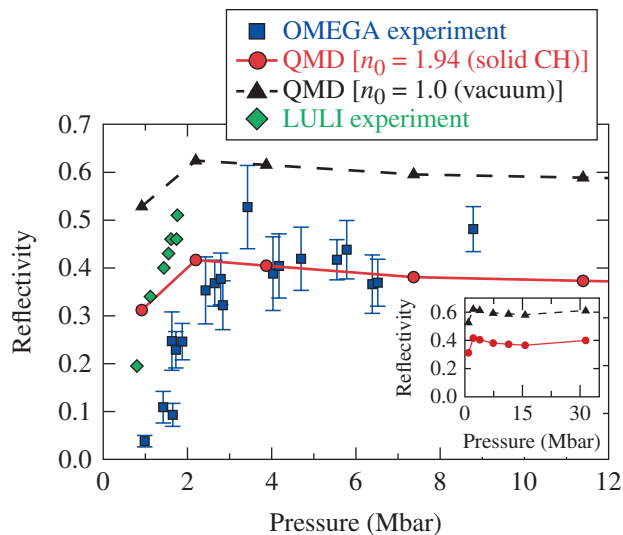
$$\begin{aligned} n(\omega) &= \sqrt{\frac{|\epsilon(\omega)| + \epsilon_1(\omega)}{2}}, \\ k(\omega) &= \sqrt{\frac{|\epsilon(\omega)| - \epsilon_1(\omega)}{2}}. \end{aligned} \quad (4)$$

Finally, the reflectivity is defined in the following general way:

$$R(\omega) = \frac{[n(\omega) - n_0]^2 + k(\omega)^2}{[n(\omega) + n_0]^2 + k(\omega)^2}, \quad (5)$$

where n_0 is the refraction index of the ambient. The choice of $n_0 = 1$ is often seen in textbooks, where the ambient is assumed to be vacuum or air. In the shock experiments, however, the reflectivity was measured as the shock propagated into the unshocked CH foil. The light reflection occurs at the interface between shocked and unshocked CH. Therefore, one must choose n_0 to be the refraction index of the unshocked CH, which was calculated to be $n_0 = 1.94$ in our QMD simulation of solid CH at room temperature. With this value of $n_0 = 1.94$, the resulting QMD reflectivity of CH shock is compared with both the OMEGA experiment²⁵ and the LULI measurement²³ in Fig. 138.46. The saturation level of the reflectivity predicted by the present QMD calculations agrees well with experiments. The turn-on of reflectivity ~ 1 to 2 Mbar is in closer agreement with the LULI experiment but seems to appear earlier than for the OMEGA experiment. If we improperly choose $n_0 = 1$, the results (black triangles) overestimate the reflectivity from $\sim 40\%$ to $\sim 60\%$. The overestimated reflection level of $\sim 60\%$ was exactly the same as what was seen in the previous QMD calculation by Wang *et al.*⁴² The inset in Fig. 138.46 plots the reflectivity for a wider range of pressures, and the reflectivity appears to be slowly increasing beyond 15-Mbar pressures, similar to the behavior seen in shocked deuterium^{18,49} occurring at $P \sim 2.8$ Mbar.

In summary, we have performed first-principles calculations for the principal Hugoniot of CH, using the QMD method. The



TC11155JR

Figure 138.46

The reflectivity of shocked CH pressure for VISAR light at $\lambda = 532$ nm along the principal Hugoniot. The QMD results, using the proper n_0 of unshocked CH (red circles) and the improper vacuum n_0 (black triangles), are compared with the LULI measurement²³ and the recent OMEGA experiment.²⁵ The inset shows the reflectivity in the entire pressure range.

QMD results agree very well with the pressure and temperature measurements up to $P = 10$ Mbar. In this pressure range, the *SESAME* model (*SESAME 7593*) predicted a similar pressure but slightly overestimated the shock temperature. For high-pressure regimes ($P = 10$ to 62 Mbar), the QMD-predicted shock temperature is higher than suggested by the *SESAME* model, thereby resulting in a stiffer CH shock in QMD simulations. Moreover, the QMD-predicted reflectivity of shocked CH agrees with a recent OMEGA experiment once the correct refraction index of the ambient (unshocked CH) is taken into account. It was found that the reflectivity starts to turn on at a somewhat smaller pressure than the recent experiment on OMEGA but appears to be closer to the LULI experiment. These results might stimulate more-accurate experiments at the high-pressure regime. Precise EOS and opacity tables based on these results could benefit fine tuning future ICF designs.

ACKNOWLEDGMENT

This material is based upon work supported by the Department of Energy National Nuclear Security Administration under Award Number DE-NA0001944, the University of Rochester, and the New York State Energy Research and Development Authority. The support of DOE does not constitute an endorsement by DOE of the views expressed in this article. This work was also supported by Scientific Campaign 10 at the Los Alamos National Laboratory, operated by Los Alamos National Security, LLC for the National Nuclear Security Administration of the U.S. Department of Energy under Contract No. DE-AC52-06NA25396.

REFERENCES

1. N. C. Santos, W. Benz, and M. Mayor, *Science* **310**, 251 (2005); A. Burrows, *Nature* **433**, 261 (2005); W. J. Borucki *et al.*, *Science* **327**, 977 (2010); S. Seager, *Science* **340**, 577 (2013).
2. G. Fontaine, P. Brassard, and P. Bergeron, *Publ. Astron. Soc. Pac.* **113**, 409 (2001).
3. B. A. Hammel *et al.*, *High Energy Density Phys.* **6**, 171 (2010).
4. K. Widmann *et al.*, *Phys. Rev. Lett.* **92**, 125002 (2004); A. Benuzzi-Mounaix *et al.*, *Phys. Rev. Lett.* **107**, 165006 (2011).
5. S. W. Haan, J. D. Lindl, D. A. Callahan, D. S. Clark, J. D. Salmonson, B. A. Hammel, L. J. Atherton, R. C. Cook, M. J. Edwards, S. Glenzer, A. V. Hamza, S. P. Hatchett, M. C. Herrmann, D. E. Hinkel, D. D. Ho, H. Huang, O. S. Jones, J. Kline, G. Kyrala, O. L. Landen, B. J. MacGowan, M. M. Marinak, D. D. Meyerhofer, J. L. Milovich, K. A. Moreno, E. I. Moses, D. H. Munro, A. Nikroo, R. E. Olson, K. Peterson, S. M. Pollaine, J. E. Ralph, H. F. Robey, B. K. Spears, P. T. Springer, L. J. Suter, C. A. Thomas, R. P. Town, R. Vesey, S. V. Weber, H. L. Wilkens, and D. C. Wilson, *Phys. Plasmas* **18**, 051001 (2011).
6. D. D. Meyerhofer, R. L. McCrory, R. Betti, T. R. Boehly, D. T. Casey, T. J. B. Collins, R. S. Craxton, J. A. Delettrez, D. H. Edgell, R. Epstein, K. A. Fletcher, J. A. Frenje, Y. Yu. Glebov, V. N. Goncharov, D. R. Harding, S. X. Hu, I. V. Igumenshchev, J. P. Knauer, C. K. Li, J. A. Marozas, F. J. Marshall, P. W. McKenty, P. M. Nilson, S. P. Padalino, R. D. Petrasso, P. B. Radha, S. P. Regan, T. C. Sangster, F. H. Séguin, W. Seka, R. W. Short, D. Shvarts, S. Skupsky, J. M. Soures, C. Stoeckl, W. Theobald, and B. Yaakobi, *Nucl. Fusion* **51**, 053010 (2011); R. L. McCrory, R. Betti, T. R. Boehly, D. T. Casey, T. J. B. Collins, R. S. Craxton, J. A. Delettrez, D. H. Edgell, R. Epstein, J. A. Frenje, D. H. Froula, M. Gatu-Johnson, V. Yu. Glebov, V. N. Goncharov, D. R. Harding, M. Hohenberger, S. X. Hu, I. V. Igumenshchev, T. J. Kessler, J. P. Knauer, C. K. Li, J. A. Marozas, F. J. Marshall, P. W. McKenty, D. D. Meyerhofer, D. T. Michel, J. F. Myatt, P. M. Nilson, S. J. Padalino, R. D. Petrasso, P. B. Radha, S. P. Regan, T. C. Sangster, F. H. Séguin, W. Seka, R. W. Short, A. Shvydky, S. Skupsky, J. M. Soures, C. Stoeckl, W. Theobald, B. Yaakobi, and J. D. Zuegel, *Nucl. Fusion* **53**, 113021 (2013).
7. L. Caillaud, S. Mazevet, and P. Loubeyre, *Phys. Rev. B* **83**, 094101 (2011).
8. L. Caillaud *et al.*, *Phys. Rev. Lett.* **107**, 115004 (2011).
9. P. Loubeyre, S. Brygoo, J. Eggert, P. M. Celliers, D. K. Spaulding, J. R. Rygg, T. R. Boehly, G. W. Collins, and R. Jeanloz, *Phys. Rev. B* **86**, 144115 (2012).
10. S. X. Hu, B. Militzer, V. N. Goncharov, and S. Skupsky, *Phys. Rev. Lett.* **104**, 235003 (2010).
11. S. X. Hu, B. Militzer, V. N. Goncharov, and S. Skupsky, *Phys. Rev. B* **84**, 224109 (2011).
12. M. A. Morales *et al.*, *High Energy Density Phys.* **8**, 5 (2012).
13. J. Vorberger, D. O. Gericke, and W. D. Kraeft, *High Energy Density Phys.* **9**, 448 (2013).

14. V. V. Karasiev *et al.*, Phys. Rev. B **88**, 161108 (2013).
15. S. X. Hu, V. A. Smalyuk, V. N. Goncharov, J. P. Knauer, P. B. Radha, I. V. Igumenshchev, J. A. Marozas, C. Stoeckl, B. Yaakobi, D. Shvarts, T. C. Sangster, P. W. McKenty, D. D. Meyerhofer, S. Skupsky, and R. L. McCrory, Phys. Rev. Lett. **100**, 185003 (2008).
16. V. Recoules *et al.*, Phys. Rev. Lett. **102**, 075002 (2009).
17. C. E. Starrett *et al.*, Phys. Plasmas **19**, 102709 (2012).
18. S. X. Hu, L. A. Collins, T. R. Boehly, V. N. Goncharov, and S. Skupsky, Phys. Rev. E **89**, 043105 (2014).
19. S. P. Marsh, ed. *LASL Shock Hugoniot Data*, Los Alamos Series on Dynamic Material Properties (University of California Press, Berkeley, CA, 1980).
20. R. Cauble *et al.*, Phys. Plasmas **4**, 1857 (1997).
21. B. I. Bennett *et al.*, Los Alamos National Laboratory, Los Alamos, NM, Report LA-7130 (1978).
22. R. M. More *et al.*, Phys. Fluids **31**, 3059 (1988).
23. M. Koenig *et al.*, Phys. Plasmas **10**, 3026 (2003).
24. N. Ozaki *et al.*, Phys. Plasmas **16**, 062702 (2009).
25. M. A. Barrios, D. G. Hicks, T. R. Boehly, D. E. Fratanduono, J. H. Eggert, P. M. Celliers, G. W. Collins, and D. D. Meyerhofer, Phys. Plasmas **17**, 056307 (2010).
26. S. Hamel, L. X. Benedict, P. M. Celliers, M. A. Barrios, T. R. Boehly, G. W. Collins, T. Döppner, J. H. Eggert, D. R. Farley, D. G. Hicks, J. L. Kline, A. Lazicki, S. LePape, A. J. Mackinnon, J. D. Moody, H. F. Robey, E. Schwegler, and P. A. Sterne, Phys. Rev. B **86**, 094113 (2012).
27. P. M. Celliers *et al.*, Appl. Phys. Lett. **73**, 1320 (1998).
28. P. M. Celliers, D. K. Bradley, G. W. Collins, D. G. Hicks, T. R. Boehly, and W. J. Armstrong, Rev. Sci. Instrum. **75**, 4916 (2004).
29. J. G. Clérouin and S. Bernard, Phys. Rev. E **56**, 3534 (1997).
30. L. A. Collins *et al.*, Phys. Rev. B **63**, 184110 (2001).
31. M. P. Desjarlais, J. D. Kress, and L. A. Collins, Phys. Rev. E **66**, 025401 (2002).
32. M. P. Desjarlais, Phys. Rev. B **68**, 064204 (2003).
33. S. A. Bonev, B. Militzer, and G. Galli, Phys. Rev. B **69**, 014101 (2004).
34. B. Holst, R. Redmer, and M. P. Desjarlais, Phys. Rev. B **77**, 184201 (2008).
35. B. Holst, M. French, and R. Redmer, Phys. Rev. B **83**, 235120 (2011).
36. C. Pierleoni *et al.*, Phys. Rev. Lett. **73**, 2145 (1994).
37. B. Militzer and D. M. Ceperley, Phys. Rev. Lett. **85**, 1890 (2000).
38. B. Militzer *et al.*, Phys. Rev. Lett. **87**, 275502 (2001).
39. K. P. Driver and B. Militzer, Phys. Rev. Lett. **108**, 115502 (2012).
40. J. M. McMahon *et al.*, Rev. Mod. Phys. **84**, 1607 (2012).
41. T. R. Mattsson *et al.*, Phys. Rev. B **81**, 054103 (2010).
42. C. Wang, X.-T. He, and P. Zhang, Phys. Plasmas **18**, 082707 (2011).
43. G. Kresse and J. Hafner, Phys. Rev. B **47**, 558 (1993).
44. G. Kresse and J. Hafner, Phys. Rev. B **49**, 14251 (1994).
45. G. Kresse and J. Furthmüller, Phys. Rev. B **54**, 11169 (1996).
46. J. P. Perdew, K. Burke, and M. Ernzerhof, Phys. Rev. Lett. **77**, 3865 (1996); J. P. Perdew, K. Burke, and M. Ernzerhof, Phys. Rev. Lett. **78**, 1396 (1997).
47. M. D. Knudson and M. P. Desjarlais, Phys. Rev. Lett. **103**, 225501 (2009).
48. R. Kubo, J. Phys. Soc. Jpn. **12**, 570 (1957); D. A. Greenwood, Proc. Phys. Soc. Lond. **71**, 585 (1958).
49. L. A. Collins, J. D. Kress, and D. E. Hanson, Phys. Rev. B **85**, 233101 (2012).